PAPER

From neurovascular coupling to neurovascular cascade: a study on neural, autonomic and vascular transients in attention

To cite this article: V Bari *et al* 2012 *Physiol. Meas.* **33** 1379

View the article online for updates and enhancements.

From neurovascular coupling to neurovascular cascade: a study on neural, autonomic and vascular transients in attention

V Bari[1,4]**, P Calcagnile**[1,4]**, E Molteni**[1]**, R Re**[2]**, D Contini**[2]**, L Spinelli**[3]**,
M Caffini**[2]**, A Torricelli**[2]**, R Cubeddu**[2]**, S Cerutti**[1]** and A M Bianchi**[1,5]

[1] Dipartimento di Bioingegneria, Politecnico di Milano, Piazza Leonardo da Vinci 32,
I-20133 Milan, Italy
[2] Dipartimento di Fisica, Politecnico di Milano, Piazza Leonardo da Vinci 32, I-20133 Milan,
Italy
[3] IFN-CNR, Istituto di Fotonica e Nanotecnologie—CNR, Piazza Leonardo da Vinci 32,
I-20133 Milan, Italy

E-mail: annamaria.bianchi@polimi.it

Abstract

Mental processes bring about neural, vascular and autonomic changes in
the brain cortex. Due to the different nature of these modifications, their
onsets show no synchrony and time dynamics is often strongly dissimilar.
After acquiring data from a group of 16 subjects, we estimated temporal
correlation between task and signals in order to assess possible influences
induced by an attentive task on electroencephalographic (EEG), heart rate
variability (HRV), oxy- and deoxy-haemoglobin concentration signals. We
also investigated correlations and time delays between couples of different
biological signals. This allowed for the isolation of a subgroup of subjects
showing similar tracks. Cardiac frequency and deoxy-haemoglobin signals
displayed a strong positive correlation with the task design, while EEG alpha
rhythm and oxygenation showed a negative correlation. Neural electrical
response was nearly instantaneous with respect to the task progression, and
autonomic response showed a mean delay of about 15 s and a slower
hemodynamic response (mean delay above 20 s) was finally induced. Globally,
the task elicited a cascade of responses, in which delays can be quantified.

---

[4] These authors contributed equally to the study.
[5] Author to whom any correspondence should be addressed.

1. Introduction

Neurovascular coupling refers to the relationship between local neural activity and subsequent changes in cerebral blood flow (CBF) (Roy and Sherrington 1890). Indeed, it has been shown that brain activity is associated with focal cortical hyperemia, that is, the changes of neural electrical activity are coupled with a functionally induced focal cortical hyper-oxygenation (Sheth *et al* 2004). Despite the fact that hemodynamic and electrical activities have been widely investigated individually (Uludag *et al* 2004), interesting physiological concerns could only be clarified by considering them conjointly. Unfortunately, the considerable differences existing between hemodynamic and electrical signals, their different physiological nature and time dynamics make it difficult to investigate neurovascular coupling as a whole.

Given this two-faced nature of neurovascular coupling, both electrophysiological and hemodynamic techniques are needed for investigation (Shibasaki, 2008). Despite the fact that functional magnetic resonance imaging (fMRI) is the gold standard for studying the hemodynamic transients in the brain (Attwell and Iadecola, 2002), it shows many drawbacks: it derives contrast mainly from changes in deoxy-haemoglobin because of its paramagnetic properties, it has a low temporal resolution and it cannot capture the electrical correlates of neurovascular phenomena. In this study, we used time-resolved near-infrared spectroscopy (NIRS) and electroencephalographic (EEG) techniques at the same time. NIRS is an optical technique that can detect the changes in concentration of the two blood chromophores, oxygenated and deoxygenated-hemoglobin (O_2Hb and HHb), by using two different wavelengths, chosen in the near infrared spectrum where the absorption of water and lipids by the tissues is negligible (Villringer *et al* 1994, Jöbsis 1977). EEG, on the contrary, allows us to detect the electrical activity of apical dendrites of large pyramidal neurons in the cerebral cortex, registering both tangentially and radially oriented current sources. It is well known that both measures are totally non-invasive and safe.

In previous studies, it has been demonstrated that the performance of a cognitive task involves the response of several physiological districts, such as central nervous system (CNS), autonomic nervous system (ANS) and cerebro-vascular system (CVS) (Tanida *et al* 2007, 2004, Moosman *et al* 2003, Obrig *et al* 1996). Despite the fact that the earliest studies on neurovascular coupling were designed as subsequent recordings of different modalities while repeating the same task, the simultaneous employment of different measurement techniques proved to be advantageous, as the experimental conditions are arduously controlled and reproduced among different test sessions in cognitive protocols (Telkemeyer *et al* 2011, Wallois *et al* 2011).

Literature reports a small number of studies investigating neurovascular coupling in cognitive tasks using EEG and NIRS techniques simultaneously. Obrig and his group (Koch *et al* 2008, Syré *et al* 2003, Obrig *et al* 2002) compared visually evoked potentials (VEP) with evoked NIRS signals, finding a decrease in the VEP component amplitude, closely coupled to a decrease in the amplitude of oxygenation parameters (O_2Hb, HHb). Combining EEG and NIRS measurements, Izzetoglu *et al* (2007) investigated the response to external stimuli using a cognitive visual oddball paradigm, finding an increase in ERP and oxygenation signal amplitude after the stimulus presentation, while Moosman *et al* (2003) investigated the common information shared by the two signals in the occipital cortex, working out the cross-correlation between alpha rhythm and concentration changes of HHb and finding that alpha activity is associated with metabolic deactivation. Sander *et al* (2007) found that time-resolved NIRS signals had an onset delay of about 5 s, if compared to the magneto-encephalographic (MEG) tracks. These results were calculated for MEG and time-resolved NIRS recordings and for a motor task. The study, though, was conducted on two subjects, and results were

reported for one of these two subjects only. Although preliminary, these evidences point out the slower rise and drop of the time-resolved NIRS signals, with respect to electromagnetic activations. The same research group also simultaneously monitored neuronal and vascular signal changes in patients in the sub-acute state of ischemic stroke, highlighting comparable findings (Leistner *et al* 2011).

In this study, neurovascular coupling has been induced by means of a bimodal audiovisual task of divided attention. Divided attention is the most demanding attentional process, and results in the ability to divide the attentive resources among two or more information sources or stimuli (Sarter and Turchi 2002).

This work specifically aims at clarifying the time relationship between EEG and hemodynamic correlates of neurovascular coupling, and at quantifying the degree of information shared by EEG and NIRS O_2Hb and HHb signals during a divided attention task involving visual and auditory resources. In order to obtain further information about the hemodynamic response and to study the activation of the ANS elicited by the execution of the cognitive task, an additional electrocardiographic (ECG) derivation was recorded.

2. Material and methods

2.1. Subjects

Sixteen healthy volunteers (eight males, eight females) took part in the present study. Mean age was 25.63 (SD 3.81 years, age range 19–34 years) and all the subjects were self-reported right handed. None of them had a lifetime or family history of cardiovascular, neurological or psychiatric illness, and all of them were declared normal for vision and hearing. They were not paid for their participation. Written informed consent was signed by all volunteers after the examination and test procedure had been explained.

2.2. Test of divided attention

The divided attention test (TDA) used in this study is a modified version of the computerized attention test battery developed by Zimmermann and Fimm (1992). Because of the outstanding behavioral results obtained by subjects undergoing the original version (results reported in Loose *et al* (2003)), the original test was modified in order to increase its difficulty. Correctness was set at 95% for the behavioral performance of a population of 16 healthy volunteers, comparable for age and education. The modified test was then re-tested on a third comparable population.

The test was composed by a 86 s baseline rest period followed by five blocks of task (165 s each) alternated with four 85 s rest periods. At the end of the test, a 300 s recovery period was recorded. Each block of task was composed by 60 pairs of auditory and visual stimuli. The auditory stimulus consisted of two frequency tones, low or high (1000 or 1500 Hz). Each tone lasted 100 ms. Target auditory stimulus was represented by two tones at different frequencies. The subjects were asked to press a button (right button of mouse) with the middle finger of the right hand as quickly as possible when an auditory target stimulus was presented.

The visual stimulus consisted of 17 white crosses in a black background. The target stimulus occurred when a cross was replaced with a white circle. The subjects were asked to press a button (left button of mouse) with the right forefinger to recognize it. The visual stimulus was presented simultaneously with the second frequency tone and lasted for 1.5 s. The interstimulus interval was 1.05 s. Figure 1 shows a schematic representation of the test.
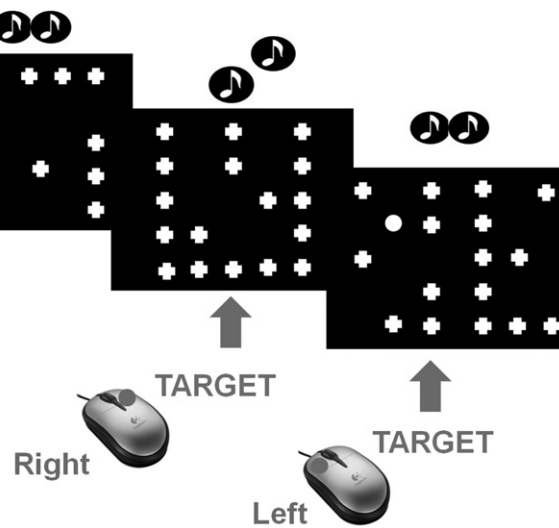
Figure 1. Schematic representation of the stimulation protocol. The visual stimulus consisted of 17 white crosses in a black background. The target stimulus occurred when a cross was replaced with a white circle. The auditory stimulus consisted of two frequency tones, low or high. The target auditory stimulus was represented by two tones of different frequencies.

Each block of tasks was composed by five target visual or auditory stimuli and 55 non-target stimuli. Target auditory and visual stimuli were never presented at the same time.

The test was presented on a computer screen using the software Presentation (Neurobehavioral Systems Inc, Albany, CA) and the subjects were provided with earphones in order to hear the frequency tones without interference from ambient sound.

2.3. Acquisition setup

2.3.1. EEG and ECG acquisition. A 19 channels EEG was recorded with Ag/AgCl electrodes placed according to the international 10/20 system (Jasper, 1958). Common ground was used as reference. Two additional bipolar electrodes were used for the collection of eye movements (EOG), and other two bipolar electrodes were placed on the chest of the subjects to collect the ECG signal. All the EEG recordings were performed by means of a 32-channel ac/dc amplifier (SAM-32, Micromed, Italy) and its data acquisition software (QuickBrain System). The A/D sampling rate was 256 Hz. Each electrode impedance was kept below 5 KΩ.

2.3.2. NIRS acquisition. A couple of pulsed diode lasers, operating at 690 and 829 nm, with 80 MHz repetition rate and <1 mW overall average power was used as a light source. The laser heads were connected to multimode graded index fibers (50/125 μm) by means of a custom-made coupler which combines a neutral density attenuator, with variable attenuation in the range 0–80 dB, and a standard FC fiber optics coupler. A stepper motor was used to automatically control the variable attenuator. Before going into the sample, light pulses passed through the optical 2 $\times$ 2 switch. Two acquisition channels were thus available. The time-resolved reflectance curves were detected by fast photomultipliers and acquired by time-correlated single photon counting (TCSPC) boards. The system was provided also with suitable probes (made of Velcro stripes and custom-made plastic holders) for positioning of
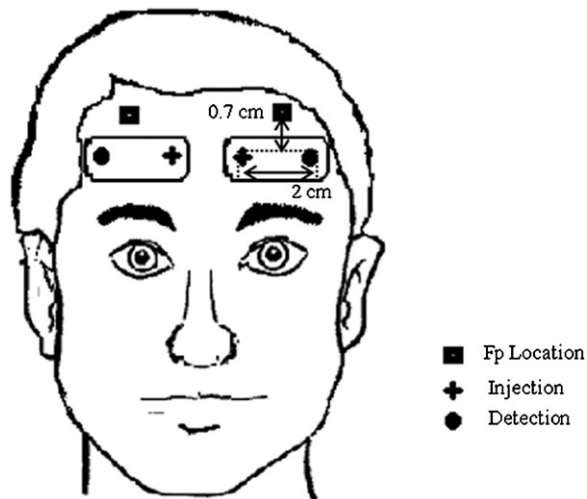
Figure 2. Example of the acquisition of NIRS signals. The sensor is positioned on the forehead of the patient, with an interfiber distance of 2 cm. The upper fiber is positioned 0.7 cm under the Fp1 and Fp2 standard locations.

the injection fibers and of the detection bundles (2 cm inter-fiber distance) on the forehead tissue, 0.7 cm under the Fp1 and Fp2 standard locations. An example of the positioning of the acquisition probe can be found in figure 2.

A detailed description and characterization of the system can be found in Re *et al* (2010). The acquired signals were sampled at 1 Hz.

2.4. Synchronization

The previously described instruments have been synchronized so that signals start to get recorded automatically at the beginning of the test and all the signals (NIRS, EEG and ECG) and the behavioral responses recorded by Presentation software were time aligned.

2.5. EEG analysis

Raw EEG data were digitally band-pass filtered between 0.5 and 48 Hz. Then they underwent Laplacian surface operator for the improvement of the spatial localization of neuronal activity, according to the method described in Foffani *et al* (2004). The data were then cleaned from ocular and muscular artifacts by means of independent component analysis (ICA) (Makeig *et al* 1996) and downsampled at 128 Hz.

The EEG frequency analysis was then performed through an autoregressive (AR) batch model estimated according to the Yule–Walker procedure. The AR estimation was performed on the electrode Fz with time windows of 2 s length with 50% overlap, in order to obtain a stationary signal. Each estimation underwent Anderson's test to evaluate the whiteness of the residual and the optimum order was chosen according to the Akaike information criterion. According to the method, through pole estimation, the spectrum is divided into bell-shaped curves and the characteristics of power and frequency of each spectral component are extracted from the position and residual of each pole. The calculation of spectral power was made following the procedure described by Zetterberg (1969) (see also Baselli *et al* 1987). The
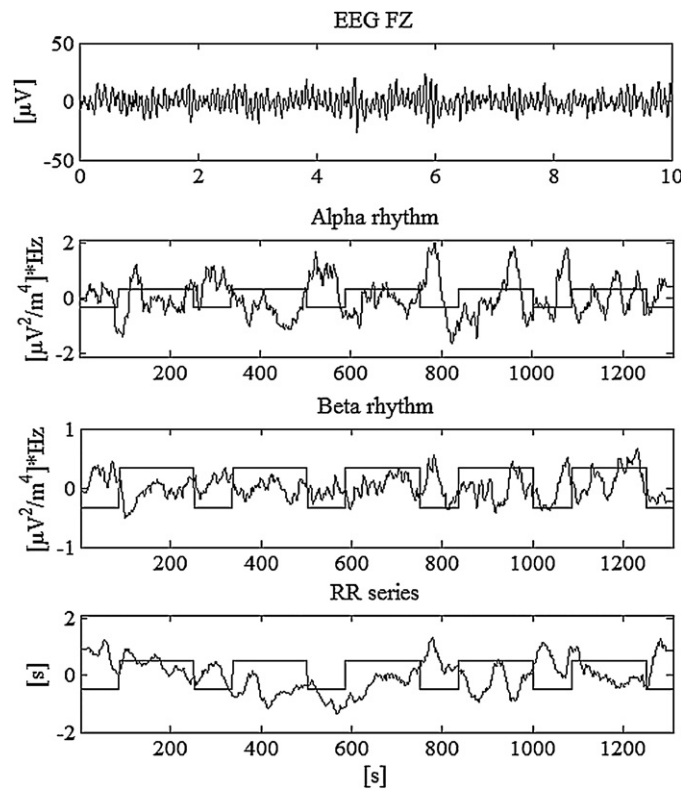
Figure 3. From top: raw EEG signal, 10 s duration; power of alpha and beta rhythm; RR series. For all the signals except the first one the whole time course during the task is presented. The square wave overlapped to the signals represents the block task. The signals are shown for subject 01.

spectral peaks were divided, according to their central frequency, into the characteristic EEG rhythms (0.5–3 Hz delta, 3–8 Hz theta, 8–13.5 Hz alpha, 13.5–30 Hz beta, 30–48 Hz low gamma).

The chosen time window length leads us to obtain one power value for each second, so that the EEG power signal could be directly compared and correlated with the NIRS signal.

2.6. RR series

From the ECG bipolar derivation acquired simultaneously with the EEG signal the inter-beat interval (RR) series were extracted by means of Pan and Tompkins' algorithm (Pan and Tompkins, 1985). The RR series were then interpolated through spline functions and resampled in order to obtain one value per second of activity, and to have the same sampling rate of EEG and NIRS signals.

An example of the acquired signals can be observed in figure 3. The reader should note that in the top panel an example of the raw EEG signal is presented within an interval of 10 s, while the other panels show the whole time course of the signals during the task.

2.7. NIRS signals analysis

2.7.1. Preprocessing: extraction of intra- and extra-cerebral NIRS signals. For each wavelength λ, a reference time domain NIRS curve $R_0(t; \lambda)$ is derived by averaging the two tracks recorded from each subject during the initial baseline period. Fitting of $R_0(t; \lambda)$ yields the reference absorption value $\mu_{a0}(\lambda)$. Then, at each recording time T during the experiment, changes in the absorption coefficient are derived as

$$\Delta\mu_a(\lambda; T) = -\frac{1}{vt} \ln\left(\frac{R(t; \lambda; T)}{R_0(t; \lambda)}\right),\tag{1}$$

where v is the speed of light in the medium, t is the arrival time of photon, and $R(t, \lambda, T)$ is the time-domain fNIRS curve at the recording time T (Nomura *et al* 1997).

   To enhance the contribution from deep layers and to remove possible disturbances caused by superficial layers, a correction method based on the use of late time windows ($t = 1750$–2500 ps) is also applied (Contini *et al* 2007). It is well known that depth information in time-domain NIRS is encoded in the time-of-flight of photons (Steinbrink *et al* 2001, Del Bianco *et al* 2002, Selb *et al* 2005, Aletti *et al* 2012). Early photons, located in the first part of the time-of-flight distribution curve, have a low probability of having reached the brain cortex, and then correspond to the oxygenation of superficial layers of the head (contributing, thus, to extra-cerebral NIRS signal); on the other hand, late photons, received in the tail of the time-of-flight distribution curve, have a higher probability to have visited deeper layers, giving rise to an intra-cerebral NIRS signal. Finally, the absorption coefficient is derived from corrected late gate intensities as

$$\mu_a(\lambda; T) = \mu_{a0}(\lambda) + \Delta\mu_a(\lambda; T).\tag{2}$$

Taking the assumption that O_2Hb and HHb are the main chromophores contributing to absorption and considering the Lambert–Beer's law for two different wavelengths λ_1 and λ_2, their concentrations are derived from the relation

$$\begin{bmatrix} C_{O_2Hb} \\ C_{HHb} \end{bmatrix} = \begin{bmatrix} \varepsilon_{O_2Hb}(\lambda_1) & \varepsilon_{HHb}(\lambda_1) \\ \varepsilon_{O_2Hb}(\lambda_2) & \varepsilon_{HHb}(\lambda_2) \end{bmatrix}^{-1} \begin{bmatrix} \mu_a(\lambda_1) \\ \mu_a(\lambda_2) \end{bmatrix},\tag{3}$$

where C are the concentrations of the considered cromophores, ε are the extinction coefficients of the cromophores at the considered λ and μ_a is the absorption coefficient at the considered λ. Then, total hemoglobin content ($tHb = HHb + O_2Hb$) is calculated.

   An example of intra- and extra-cerebral NIRS signals can be observed in figure 4, comparing left and right panels.

2.7.2. Signal processing. After the observation of raw signals, two main contributions in the NIRS signals were isolated, by means of a low-pass Chebychev IIR filter with six coefficients, passband 0.002 Hz and stop band 0.003 Hz, with -30 dB below the passband maximum ripple amplitude. The phase shift was corrected to 0 for the band pass, by introducing a pure phase shift compensator for the IIR filter. This procedure preserves from erroneous delays in signals due to filtering.

   The slow component was late deemed to be due to the sustained attention condition required by the test, whereas the fast contribution was later attributed to the modulation caused by the switching between test and rest periods. An example of slow and fast components for O_2Hb and HHb signals can be observed in figure 4, if comparing top and bottom panels. The temporal trend of the task is superimposed.
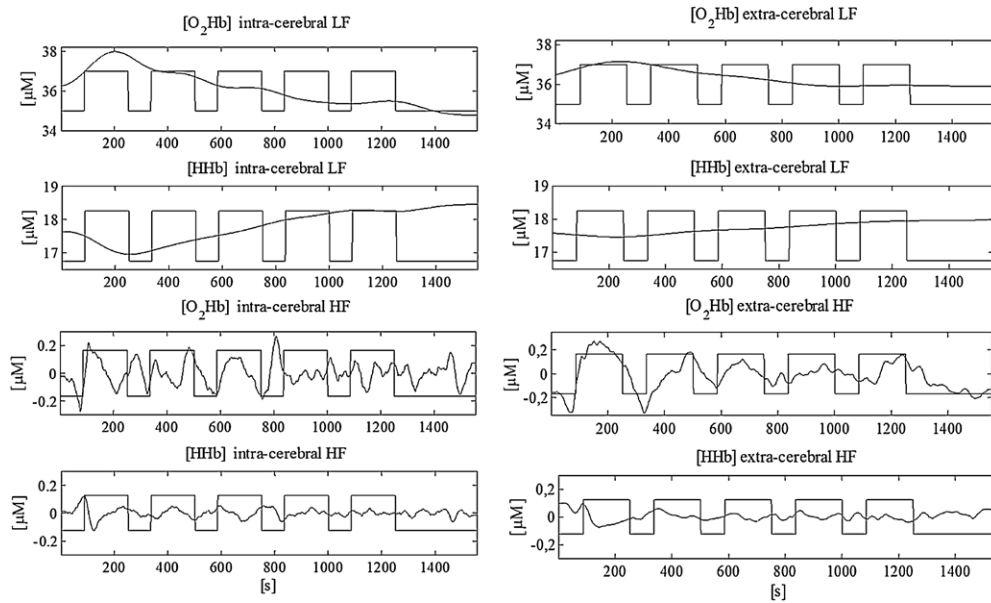
Figure 4. From top: [O₂Hb] and [HHb] slow component (top rows), [O₂Hb] and [HHb] fast component (bottom rows). Left panel: intra-cerebral signals, right panel: extra-cerebral signals. All the signals shown belong to subject 13. The temporal schema of the task is also superimposed.

2.8. Correlations

The quantification of neurovascular coupling was obtained by means of the estimation of the cross-correlation (CC) function. CC was applied, firstly, between each signal and the task, and then between pairs of signals. As shown in the upper part of table 1, CC with the task was calculated for the following signals: alpha EEG power rhythms (extracted from Fz electrode), the RR series, O₂Hb and HHb fast component from intra- and extra-cerebral NIRS signals. The task was modeled as a square wave: test intervals corresponded to high values, while rest periods corresponded to low values. Initially, the correlation of beta power rhythm with the task was evaluated as well, but the results were then excluded from the discussion as explained in 3.2.

Then CC was evaluated between pairs of signals: alpha power rhythm—RR series, alpha power rhythm—fast O₂Hb and HHb intra-cerebral signals, RR series—fast O₂Hb and HHb intra- and extra-cerebral signals, as shown in the lower part of table 1.

Before undergoing correlation, all the signals (except for the task) were moving average filtered with a 29 sample window and time re-aligned, in order to reduce signal variability due to noise. All the signals were also cut in order to have all the same length (from 86 s before the beginning of the test to 60 s after its end). Normalized CC was then applied to each pair of data. CC was defined as (Orfanidis 1996)

$$\hat{R}xy(m) = \begin{cases} \sum_{n=0}^{N-m-1} x_{n+m}y_n & m \geqslant 0 \\ \hat{R}yx(-m) & m < 0 \end{cases}, \tag{4}$$

where x_n and y_n are stationary random processes.

Table 1. Real CC and CC_{100} results

Signals[a]	Real CC[b] (mean $\pm$ SD), $p \ll 0.001$	CC_{100} surrogates[c]t (mean $\pm$ SD), $p \ll 0.001$	% signals outstandig confidence interval[d] $M_n \pm 1.96 \cdot$ SD
Alpha–task	-0.26 ± 0.15	0.0002 ± 0.004	93.75%
RR series–task	-0.48 ± 0.20	0.0031 ± 0.007	100%
O_2Hb intra-cerebral–task	-0.36 ± 0.13	0.0024 ± 0.004	93.75%
HHb intra-cerebral–task	0.35 ± 0.19	0.0006 ± 0.005	96.88%
Alpha–RR series	0.20 ± 0.09	-0.0011 ± 0.006	87.5%
Alpha–O_2Hb intra-cerebral	0.21 ± 0.11	0.0004 ± 0.004	93.75%
Alpha–HHb intra-cerebral	-0.25 ± 0.18	0.0025 ± 0.005	87.5%
RR–O_2Hb intra-cerebral	0.37 ± 0.15	-0.0002 ± 0.005	96.88%
RR–HHb intra-cerebral	-0.28 ± 0.2	-0.0010 ± 0.007	100%
RR - O_2Hb extra-cerebral	0.23 ± 0.23	-0.0017 ± 0.0042	100%
RR–HHb extra-cerebral	-0.15 ± 0.24	0.0002 ± 0.0058	100%

[a] Pair of the signal for which the CC have been calculated. It should be pointed out that correlations that include NIRS signals are made for both left and right pads, doubling the number of evaluated CC.
[b] Mean value of CC for pair of signals in [a] evaluated over the eight subjects identified (see 3.5).
[c] Mean value of CC_{100} for pair of signals in [a].
[d] Percentage of subjects for which real CC was outside the confidence interval ($M_n \pm 1.96 \cdot$ SD). Values in [d] are calculated over all the 16 subjects. All results are shown in terms of mean $\pm$ SD, all p-values of the CC for each subject were reported as $\ll 0.001$.

The obtained CCs are given in a length $2 \cdot$ N-1 vector, where x and y are length N vectors ($N > 1$):

$$c(m) = Rxy(m - N), \quad m = 1, \ldots, 2N - 1. \tag{5}$$

CC was then normalized by N as

$$R_{xy,\text{biased}}(m) = \frac{1}{N} R_{xy}(m). \tag{6}$$

The temporal shift m between each pair of signals for which the CC maximum absolute value was reached, within one task period, was considered; $c(m)$ was then extracted and the corresponding p-value was calculated. Depending on the pair of signals under processing, a maximum or minimum value of correlation was considered.

2.9. Significance of CC

Results for all the CCs computed between pairs of signals were compared with values obtained from a surrogate analysis. In different surrogate series, being $n = 100$, were obtained by randomizing the values of the signal across time (i.e. by shuffling the samples of the signal, and thus preserving its length, mean and SD).

This analysis was conceived for testing the significance of CC between each signal and the task (by creating surrogates of the considered physiological signal) and also for testing the significance of CC between pairs of signals (by randomizing alternatively one of the two signals).

Assuming a normal distribution of the CC of surrogate data, the confidence interval at 95% has been calculated as $M_n \pm 1.96 \cdot SD_n$ on the 100 different realizations. If the value of CC calculated on real signals resulted external to this interval (that means CC lower than $M_n - 1.96 \cdot SD_n$ or higher than $M_n + 1.96 \cdot SD_n$), the CC was considered significant.

In order to achieve a robust estimate of M_n, the number of iterations n was chosen to be equal to 100, and correspondingly the notation CC_{100} is used. Results can be examined in figure 5 for all the subjects.
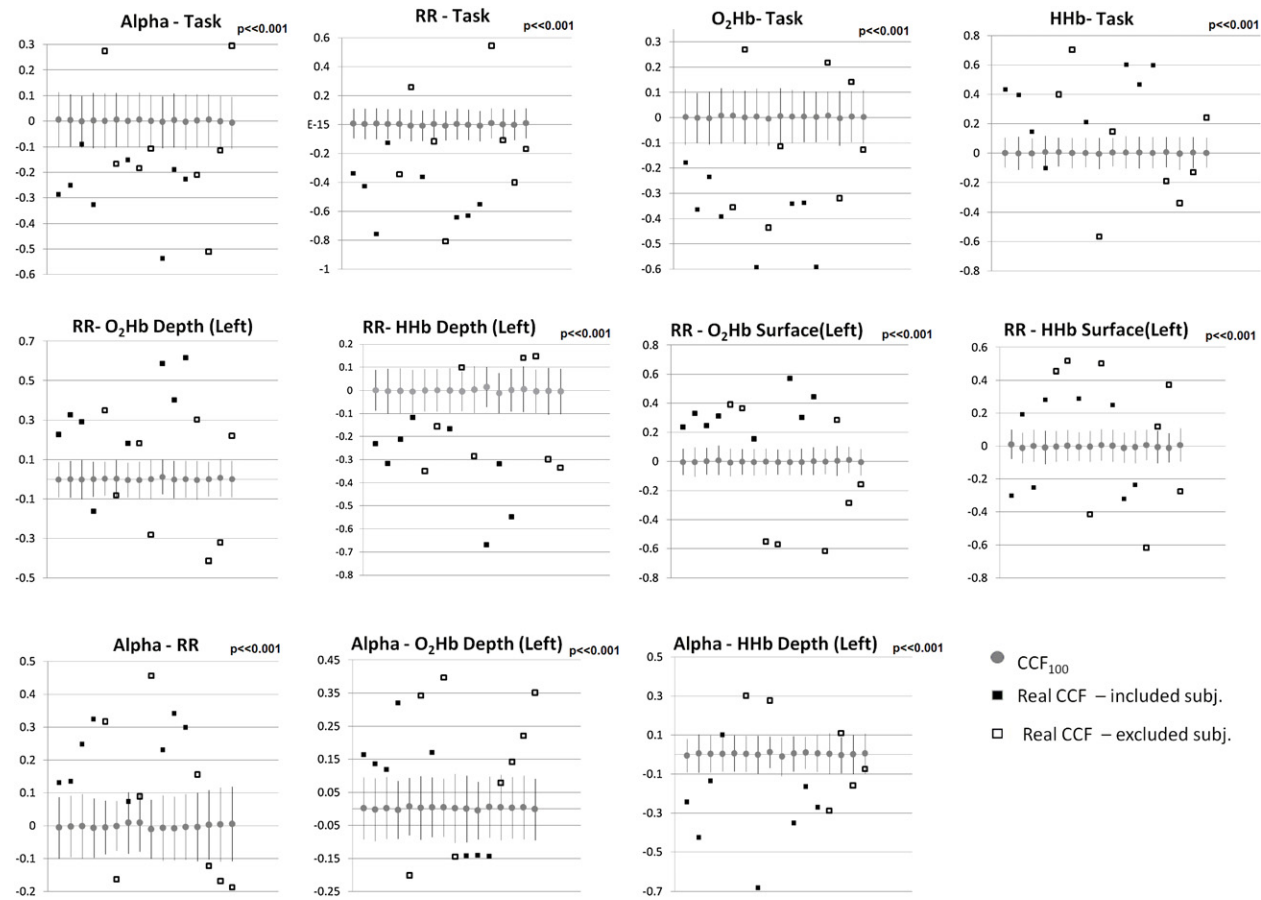
Figure 5. Results of CC evaluated on all the pairs of signals and for each subject compared to the CC_{100} obtained from surrogated data (see text for details). In each panel, gray circles represent, for all the subjects, mean $\pm$ 1.96 · SD of 100 surrogate correlations (i.e. CC_{100}), while squares indicate real CC between the signals indicated for each subject. Black squares indicate subjects who, having a similar trend of CC, have been included in the group for which mean results are presented (see 3.5) and white squares indicate subjects excluded from this group. For CCs that include NIRS signals, only results derived by left pad are presented, but results from the right one are similar.

An additional statistical analysis was carried out using a two-tailed paired *t*-test to attest the significance of the difference in the distribution among the real CC values and CC_{100} surrogate values (that is the mean of the 100 surrogate correlations for each subject). For each pair of signals, the mean CC across subjects was compared with the mean CC_{100}. *P*-values of this *t*-test are reported in figure 5 and all resulted $\ll 0.001$.

3. Results

3.1. Behavioral results

The 16 subjects committed an average of 0.13 ± 0.49 Visual Omission errors (0.13 missing answers on 15 visual target stimuli, corresponding to 1.18% error), 0.47 ± 0.63 Auditory Omission errors (0.47 missing answers on 15 auditory target stimuli, corresponding to 3.53% error) and 11.63 ± 24.42 Commission errors (all kinds), corresponding to 11.63 wrong answers (3.89%) during the entire divided attention test. They answered to the visual target stimuli in 649.55 ± 129.27 ms and to the auditory target stimuli in 698.14 ± 141.30 ms.

3.2. EEG results

The correlation between alpha rhythm and the task, modeled as a square wave, showed in general negative values (14 out of 16 subjects). Indeed, Alpha power increased for this group of subjects during the resting periods. The mean CC value among these subjects was -0.23 ± 0.17, $p \ll 0.001$.

The correlation between beta rhythm and the task showed positive values for eight subjects and negative values for the other eight. Even though for 14 subjects out of 16 the mean delay of beta rhythm with respect to the task resulted lower than 1 s, which is a plausible time for the neuronal response onset, the different behavior over the subjects made it impossible to identify a prevalent trend. Beta rhythm was then excluded from the subsequent analysis.

3.3. RR series results

The RR series showed a strong modulation related to the cognitive task, also confirmed by values of CC. An increasing trend of beat-to-beat interval throughout the whole test was put into evidence, meaning that the cardiac frequency, after an increase at the beginning of the test, slowly tends to recover to the baseline values. The series was then linearly detrended before calculating the CC, to avoid erroneous results due to the presence of the slow component.

Correlation with the task was negative for 14 out of 16 subjects (implying that the RR period decreased during test periods and increased during the resting periods), with a mean value of -0.41 ± 0.24, $p \ll 0.001$.

3.4. NIRS results

The slow components of [O_2Hb] and [HHb] intra-cerebral signals were characterized by an increase of [O_2Hb] and a decrease of [HHb]. This trend in some cases lasted until the end of the test (six subjects for the right pad, five for the left one for O_2Hb, four subjects for both the right and left pads for HHb), while, in other cases, after an initial increase of O_2Hb/decrease of HHb, it showed a recovery toward the initial values (10 subjects for the right pad, 11 for the left one for O_2Hb and 12 subjects for the left and right pads for HHb). An example of the latter case can be observed in figure 4.

Considering the tracks of both O_2Hb and HHb intra-cerebral signals, three different time courses were observed.

1. *Opposite trend (eight subjects for the right pad and seven for the left pad)*. This means that an increase in $[O_2Hb]$ and a decrease in $[HHb]$, or an opposite recovery.

2. *Similar trend (four subjects for the right pad and four for the left pad)*. This means that both the signals increased, decreased, or had the same kind of recovery.

3. Different trend (neither opposite, nor similar, four subjects for the right pad and five for the left pad) of the $[O_2Hb]$ and $[HHb]$ signals.

The extra-cerebral signals showed the same trends as the intra-cerebral, but it was not possible to work out a classification based on the observation of the two $[O_2Hb]$ and $[HHb]$ signals together, because of their large variability among the subjects.

After removing the slow component trough a high-pass filter (see the method in section 2.7.2), the CC between signals and task was estimated only for the fast components of the NIRS signals, both in intra- and extra-cerebral signals, as the task modulated only these ones. All the p-values of the estimation resulted $p \ll 0.001$.

The correlation between the O_2Hb intra-cerebral signals and the square wave task showed a negative trend for 15 subjects on the right pad and 13 on the left one.

Mean values of CC minima were, respectively, -0.26 ± 0.14 and -0.34 ± 0.15, with an average between the two pads of -0.30 ± 0.15.

The correlation between the HHb intra-cerebral signals and the square wave task showed positive values for 13 subjects on the right pad and 10 on the left. The mean value of CC maxima was, respectively, 0.27 ± 0.15 and 0.41 ± 0.19, with an average between the two pads of 0.33 ± 0.23. All the CC between NIRS signals and task were significantly different from surrogate data as shown in figure 5.

The correlation between O_2Hb extra-cerebral signals and the task was negative for nine subjects on the right pad and 11 on the left, but it was inverted (e.g. negative for the right pad and positive for the left pad or vice versa) on the two pads of six subjects. The correlation between the HHb extra-cerebral signals had a different sign on the two pads for almost half of the subjects. It showed positive values for only half of the subjects on the right pad and 10 on the left.

All the CCs between NIRS extra-cerebral signals and the task showed contrasting results and large variability among the subjects and between the two pads of the same subject, with respect to the intra-cerebral signal. No evident interrelation between NIRS extra-cerebral data and the task was found for the subjects. For this reason, correlations between $[O_2Hb]$ and $[HHb]$ NIRS extra-cerebral signals and the task were considered not reliable and their results will not be presented and further discussed in the following sections.

3.5. Identification of a group of subject

Figure 6 shows the grand average of signals (EEG alpha and beta rhythms, $[O_2Hb]$ and $[HHb]$ NIRS intra-cerebral signals, RR series) acquired from all the 16 subjects.

From the observation of the correlations mentioned above, a group of eight subjects (50% of the investigated population) showing similar correlations was identified. These subjects correspond to the identification codes 01, 04, 05, 07, 10, 14, 15, 16.
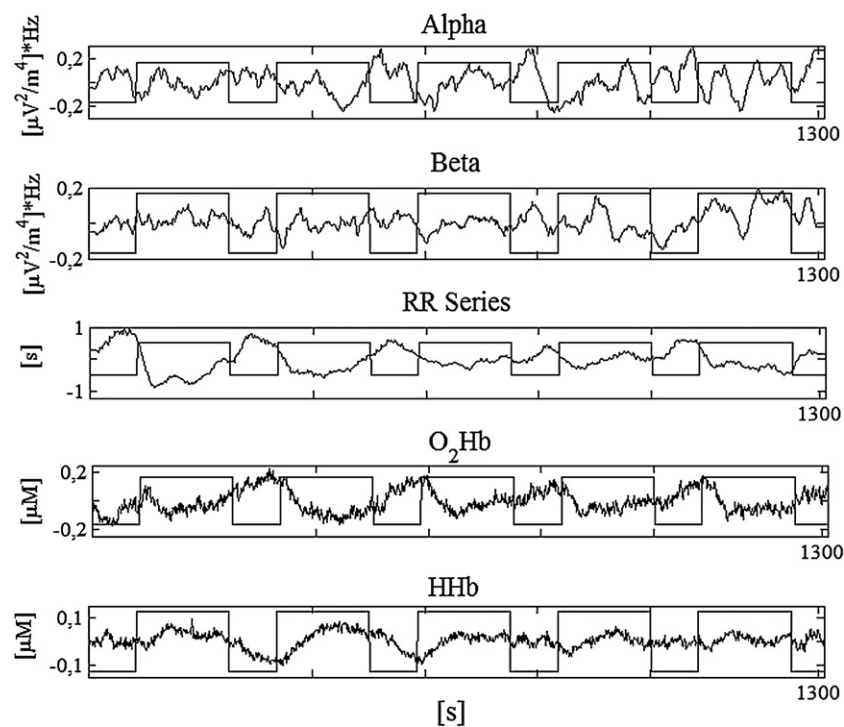
Figure 6. Grand averages of all the acquired signals from all the subjects. From top: power of alpha and beta rhythm, RR series, concentration of O_2Hb and HHb intra-cerebral signals.

3.6. CC results

Table 1 summarizes the results of CC of both real signals and surrogates, for all the pairs of signals for which it was computed. Results are presented as mean values of the eight subjects included in the group described above.

In the upper part of the table, results concerning correlations with the task are presented, while in the lower part results of CCs over pairs of signals are shown.

CC with the task resulted negative for alpha rhythm, RR series and [O_2Hb] and positive for [HHb]. The signs of the CCs were always found to be consistent with the observations (e.g. if alpha and RR are correlated in a negative way with the task, then the correlation between them resulted positive).

Considering the surrogate series generated for each signal of each subject, it was found that, for each signal, for almost all the 16 subjects, the real CC values fall outside the null hypothesis interval provided by $CC_{100} \pm 1.96 \cdot SD$ as shown in figure 5 and table 1.

This additional analysis allowed us to rule out that the resulting correlation values could be due to a causal relation among the investigated processes.

The mean delay between each signal and the task was then evaluated in order to identify the response delay of each physiological district (neuronal, systemic, hemodynamic) with respect to the divided attention task. As explained above, the beta signal was excluded from this analysis, as well as superficial NIRS data. Alpha rhythm showed a peak of correlation with the task at lag 0 for all subjects but one. Thus, all the subjects revealed synchronous dynamics for alpha rhythm and the task, with only one exception. The subject, showing the alpha delay
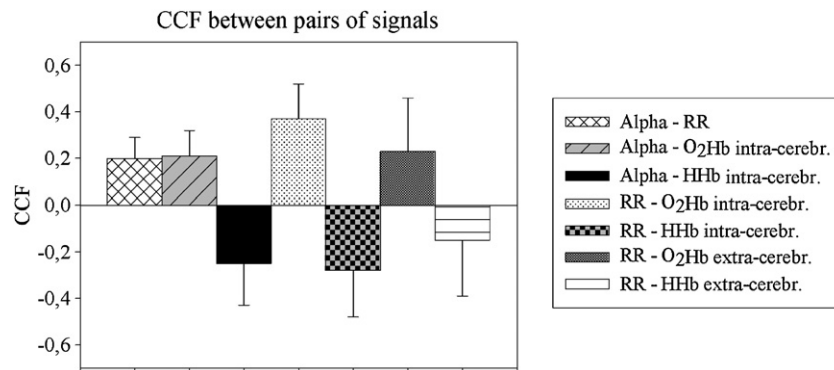
Figure 7. Mean values of CC among pairs of signals. Correlations between alpha rhythm and intra-cerebral HHb, between RR series and intra-cerebral HHb and between RR series and extra-cerebral HHb are negative: *p*-values always $\ll 0.001$.

Table 2. Mean delay between each signal and the task.

Signals[a]	Delay[b] (s)
Alpha–task	0.00 ± 0.50
RR series–task	15.75 ± 14.02
O_2Hb–task	19.69 ± 21.27
HHb–task	34.43 ± 30.25

[a] Pair of signals for which the CC results have been calculated.
[b] Mean delay for which a maximum or minimum of correlation occurred in terms of mean $\pm$ SD.

of 14 s and also an opposite sign of alpha–RR correlation with respect to the other subjects, was considered an outlier for the alpha correlation, and was excluded from the average. As shown in table 2, the resolution of the CC analysis was 1 s.

The delay between each signal and the task averaged over eight subjects (mean $\pm$ standard deviation) are shown in table 2. It is possible to identify a temporal cascade of responses: the activation of alpha rhythm is almost instantaneous and it is followed by RR series decrease that could be associated with a sympathetic activation. Last, NIRS signals variations are elicited, attesting the contribution of the hemodynamic activity.

The CC among pairs of signals was then calculated: alpha and RR, alpha and $[O_2Hb]$, alpha and [HHb], RR and $[O_2Hb]$, RR and [HHb]. NIRS extracerebral signals were considered only evaluating the CC with RR series. Figure 7 shows the mean results of CC ($\pm$ SD) between pairs of signals. *P*-values resulted $\ll 0.001$ for all the CCs evaluated.

Even no statistical differences were found between the CCs shown in figure 7, the highest value was found between intra-cerebral $[O_2Hb]$ and RR series followed by the correlation between intra-cerebral [HHb] and RR series. Interestingly, all of these signals share a common cardiovascular origin, which will be discussed further.

4. Discussion

While performing electrical activity, neurons come across a number of cellular processes, such as the release and recycling of neurotransmitting molecules and the regulation of trafficking through the ionic channels (Riera and Sumiyoshi, 2010). All these activities require

large energy expenditure, biologically 'translated' into a huge consumption of adenosine triphosphate (ATP). Albeit ATP can be synthesized through at least three different pathways in our body, the brain largely fosters the oxidative glucose metabolism. As this pathway is aerobic, cerebral metabolism ultimately relies on a constant supply of both glucose and oxygen. The provision of these two energy substrates is maintained by the CBF, which delivers glucose and oxygen to the neural tissue through the complex network of blood vessels in a brain vascular system. Accordingly, within some seconds after the onset of a localized neural activity, increases in oxygen and glucose consumption are followed by an increase in the CBF. The oxygen supply is larger than the concomitant increase in oxygen consumption (Fox and Raichle 1986), resulting in a local increase of oxygenated hemoglobin. The rise in the CBF is mainly achieved by arteriolar dilation inducing increased perfusion pressure downstream. Very recent observations support the hypothesis that red blood cells may act as sensors of local tissue hypoxia, through the oxygenation status of the hemoglobin, and initiate improved local perfusion to the tissue through hypoxic vasodilation (Thorn *et al* 2011). Blood flow per single capillary is increased mainly by intensification in blood flow velocity, whereas capillary recruitment, i.e. opening and closing of capillaries, seems not to occur in the brain (Göbel *et al* 1989, Villringer *et al* 1994). These factors result in a local increase in $[O_2Hb]$ and a drop in [HHb] (Obrig *et al* 1996), being the latter also the main basis of the fMRI BOLD contrast (Kwong *et al* 1992, Ogawa *et al* 1992, Frahm *et al* 1992, Bandettini *et al* 1992).

In our work, we simultaneously recorded EEG, ECG and NIRS signals during the performance of a bimodal task of divided attention. All the subjects were able to fully accomplish the attentive request, as they could complete the task providing accuracy above 95% for all the conditions. On the other hand, some errors were made, indicating that some of the subjects, but not all of them, operated at the very limit of their attentive capabilities. In general, the performances in the execution of the test (low error rates) are better than the ones usually reported in the literature (Loose *et al* 2003). This may indicate that not all the examined subjects were at the very limit of their attentive capabilities, and may explain the high variability found in the results. For this reason, in the description of the results, we selected, from the whole group of subjects, the subgroup with a similar and repeatable behavior.

The first relevant result is the major modulation induced by the attentive task on alpha EEG rhythm. Such conditioning was not observed in the beta frequency range. Our findings are in agreement with Bollimunta *et al* (2011), who found that visual attention reduces the magnitude of alpha oscillations as well as the level of alpha interactions in macaques, and Mo *et al* (2011), who suggested that ongoing alpha oscillations in inferotemporal cortex may be part of the neuronal mechanism representing task-relevant information.

The slow components of NIRS intra-cerebral signals showed, in most of the examined subjects, an increase in O_2Hb with a concurrent decrease in HHb during the first part of attention task. The reached values are sometimes maintained during all the test, sometimes a recovery toward the initial baseline is already present during the execution of the task, as explained in section 3.4. This finding is fully consistent with the previous literature (Kubo *et al* 2008, Fallgatter and Strik, 1998) and with a previous work of the research group (Butti *et al* 2009).

On the other hand, the fast components of NIRS intra-cerebral signals displayed a decrease of O_2Hb and a concurrent increase of HHb during the task blocks. This behavior, which could appear contradictory with respect to previous works on cerebral activations, is however superimposed to the slow component, and seems to account for the short-term energetic expenditure due to the alternation of task and rest periods. Indeed, the robust attentive request caused by the task prompted vast gathering of hemoglobin, clearly visible during the rest periods interleaved between the blocks, which show that O_2Hb increases and HHb decreases,

thus indicating hemoglobin accumulation. Overall, we interpreted the fast component of NIRS intra-cerebral signals as the result of the energetic modulation dictated by the block design of the task.

The lack of reliability found for the extra-cerebral contribution to NIRS signals has already been discussed elsewhere by our group (Aletti *et al* 2012), and by the recent literature (Takahashi *et al* 2011): the extra-cerebral component of NIRS signals, measured over the forehead, proved indeed to be affected by a skin blood flow contribution, in its turn dependent on systemic drive, while the deep cortical NIRS signal did not appear to be tainted by extra-cerebral vascular activity, but rather neural dynamics were dominant with respect to the autonomic control of circulation. The activity detected by the probe has been considered representative of the real hemodynamic response, without considering the possibility of a negative surrounding effect, since previous studies did not put into evidence this effect even using larger probes with a higher number of light sources and detectors and thus able to explore more extended cortical areas (Butti *et al* 2009, Molteni *et al* 2012). Surrogate data analysis confirmed that all the correlation values presented in table 1, although low in value in some cases, are statistically significant. As expected, the highest correlation values were obtained for the relationship between the RR series and the task.

Correlations between O_2Hb and the task and between HHb and the task showed high values as well. This fact suggests that the modulatory pattern captured by fast components of NIRS intra-cerebral signals was connected with the energetic request of the task. A high correlation was found between the RR series and NIRS intracerebral signals: this could reflect a common autonomic drive. On the other hand, the CC between the RR series and extracerebral signal was lower. This may be interpreted as an autonomic response to an increased energetic demand at the cortical level. Further investigations with specific tests are planned in the near future.

NIRS intra-cerebral signals displayed also good CC values with alpha rhythm: once more, this put into evidence a strong interdependence between the cognitive effort and the metabolic demand. Furthermore, the time courses of NIRS fast component intra-cerebral signals and alpha rhythm show the presence of neuronal desynchronization (reduction in alpha power), reduction in O_2Hb concentration and increase in HHb during the test period. The higher correlation between alpha rhythm and [HHb], with respect to alpha and [O_2Hb], was also reported by Moosman *et al* (2003) and may be related to the fact that neuronal activation, testified by alpha desynchronization, is mostly related to oxygen consumption, testified by the HHb increase. It is worth noting that the oscillations in HHb and O_2Hb (fast components in the NIRS signal) are superimposed to the slow NIRS components. A correlation between the RR series and alpha rhythm has also been evidenced.

Table 2 resumes the activations induced by the attention task. Activation of several systems was observed, each one characterized by a different time delay: neural electrical response was the first one (alpha rhythm dynamics with respect to the task was simultaneous), autonomic response was then risen (mean delay of RR series 15.75 s) and a slower hemodynamic response (mean delay of O_2Hb around 20 s, around 30 s for HHb) was finally induced. It should be taken into account that these delays have been quantified by averaging the response to all the five blocks of the task. Moreover, with the exception of the first block, we quantified a modulation of the activity that was already elicited since the beginning of the task. Even if the subtraction of the slow dynamics could have helped in isolating fast activation, it can be hypothesized that the rest blocks were not long enough to restore a basal condition. This fact could explain why the activation of neuronal, hemodynamic and autonomic responses was found to be much slower than other findings reported in the literature, which discussed delays with reference to pure basal situations.

Globally, it can be affirmed that the task elicited a cascade of responses, in which time delays could be quantified.

The correlations between pairs of signals showed that the different responses to the task were interdependent: a desynchronization of alpha rhythm, a reduction in O_2Hb concentration and an increase in HHb concentration and heart rate were doubtless observed during the test blocks. These phenomena mirror metabolic consumption and prove to reverse during rest periods. For these reasons, we can infer that the cognitive task is effectively the generator of the neuronal, autonomic and hemodynamic responses.

Lastly, despite the findings described above, the authors would also highlight some limitations of this work. (i) The two-channel NIRS device provided a limited head coverage, only probing the frontopolar area, (ii) the synchronous placement of EEG electrodes and NIRS emitters and receivers could not be done with respect to any standard or guidelines and (iii) signals showed high inter-subject variability, probably due to a low demanding task, which could only be handled by arbitrarily restricting the discussion to a subgroup of subjects who showed concordant results.

5. Conclusion

This work is a contribution to the study of neurovascular coupling during cognition. Activation of several systems was observed, each one characterized by a different time delay: neural electrical response was the first one, autonomic response was then raised, and a slower hemodynamic response was induced last. A cascade of responses was then identified, and delays were quantified. Importantly, we could show that the metabolic request induced by some cognitive effort in the brain is mirrored in the cardiovascular compartment: the electrocardiographic signal (or at least the inter-beat-interval series) accounts for autonomic activation, as well as the dynamics of O_2Hb and HHb which seems to bear a stronger imprinting of the energetic phenomena occurring in the brain. Nevertheless, further work is still needed for the investigation of the relationships between neural activation and vascular supply.

Acknowledgment

References

Aletti F *et al* 2012 Deep and surface haemodynamic signal from functional time resolved transcranial near infrared spectroscopy compared to skin flowmotion *Comput. Biol. Med.* **42** 282–9

Attwell D and Iadecola C 2002 The neural basis of functional brain imaging signals *Trends Neurosci.* **25** 621–5

Bandettini P A, Wong E C, Hinks R S, Tikofsky R S and Hyde J S 1992 Time course EPI of human brain function during task activation *Magn. Reson. Med.* **25** 390–7

Baselli G, Cerutti S, Civardi S, Lombardi F, Malliani M, Merri M, Pagani M and Rizzo G 1987 Heart rate variability signal processing: a quantitative approach as an aid to diagnosis in cardiovascular pathologies *Int. J. Biomed. Comput.* **20** 51–70

Bollimunta A, Mo J, Schroeder C E and Ding M 2011 Neuronal mechanisms and attentional modulation of corticothalamicα oscillations *J. Neurosci.* **31** 4935–43

Butti M, Contini D, Molteni E, Caffini M, Spinelli L, Baselli G, Bianchi A M, Cerutti S, Cubeddu R and Torricelli A 2009 Effect of prolonged stimulation on cerebral haemodynamic a time-resolved fNIRS study *Med. Phys.* **36** 4103–14

Contini D, Spinelli L, Torricelli A, Pifferi A and Cubeddu R 2007 Novel method for depth-resolved brain functional imaging by time-domain NIRS *Proc. SPIE* **6629** 662908

Del Bianco S, Martelli F and Zaccanti G 2002 Penetration depth of light re-emitted by a diffusive medium theoretical and experimental investigation *Phys. Med. Biol.* **47** 4131–44

Fallgatter A J and Strik W K 1998 Frontal brain activation during the Wisconsin card sorting test assessed with two-channel near-infrared spectroscopy *Eur. Arch. Psychiatry Clin. Neurosci.* **248** 245–9

Foffani G *et al* 2004 Independent component analysis compared to Laplacian filtering as 'deblurring' techniques for event related desynchronization/synchronization *Methods Inf. Med.* **43** 74–8

Fox P T and Raichle M E 1986 Focal physiological uncoupling of cerebral blood flow and oxidative metabolism during somatosensory stimulation in human subjects *Proc. Natl Acad. Sci. USA* **83** 1140–4

Frahm J, Bruhn H, Merboldt K D and Hänicke W 1992 Dynamic MR imaging of human brain oxygenation during rest and photic stimulation *J. Magn. Reson. Imaging* **2** 501–5

Göbel U, Klein B, Schröck H and Kuschinsky W 1989 Lack of capillary recruitment in the brains of awake rats during hypercapnia *J. Cereb. Blood Flow Metab.* **9** 491–9

Izzetoglu M, Bunce S C, Izzetoglu K, Onaral B and Pourrezaei K 2007 Functional brain imaging using near-infrared technology *IEEE Eng. Med. Biol. Mag.* **26** 38–46

Jasper H H 1958 The ten twenty electrode system of the international federation *Electroencephalogr. Clin. Neurophysiol.* **10** 371–5

Jöbsis F F 1977 Noninvasive, infrared monitoring of cerebral and myocardial oxygen sufficiency and circulatory parameters *Science* **198** 1264–7

Koch S P, Koendgen S, Bourayou R, Steinbrink J and Obrig H 2008 Individual alpha-frequency correlates with amplitude of visual evoked potential and haemodynamic response *Neuroimage* **41** 233–42

Kubo M, Shoshi C, Kitawaki T, Takemoto R, Kinugasa K, Yoshida H, Honda C and Okamoto M 2008 Increase in prefrontal cortex blood flow during the computer version trail making test *Neuropsychobiology* **58** 200–10

Kwong K K *et al* 1992 Dynamic magnetic resonance imaging of human brain activity during primary sensory stimulation *Proc. Natl Acad. Sci. USA* **89** 5675–9

Leistner S, Sander-Thoemmes T, Wabnitz H, Moeller M, Wachs M, Curio G, Macdonald R, Trahms L and Mackert B M 2011 Non-invasive simultaneous recording of neuronal and vascular signals in subacute ischemic stroke *Biomed. Tech. (Berl.)* **56** 85–90

Loose R, Kaufmann C, Auer D P and Lange K W 2003 Human prefrontal and sensory cortical activity during divided attention tasks *Hum. Brain Mapp.* **18** 249–259

Makeig S, Bell A J, Jung T P and Sejnowski T J 1996 Independent component analysis of electroencephalographic data *Adv. Neural Inf. Process. Syst.* **8** 145–151

Mo J, Schroeder C E and Ding M 2011 Attentional modulation of alpha oscillations in macaque inferotemporal cortex *J. Neurosci.* **31** 878–82

Molteni E, Contini D, Caffini M, Baselli G, Spinelli L, Cubeddu R, Cerutti S, Bianchi A M and Torricelli A 2012 Load-dependent brain activation assessed by time domain functional near-infrared spectroscopy during a working memory task with graded levels of difficulty *J. Biomed. Opt.* **17** 056005

Moosmann M, Ritter P, Steinbrink A, Thees S, Blankenburg F, Taskin B, Obrig H and Villringer A 2003 Correlates of alpha rhythm in functional magnetic resonance imaging and near infrared spectroscopy *Neuroimage* **20** 145–58

Nomura Y, Hazeki O and Tamura M 1997 Relationship between time-resolved and non-time-resolved Beer–Lambert law in turbid media *Phys. Med. Biol.* **42** 1009–23

Obrig H, Hirth C, Junge-Hülsing J G, Döge C, Wolf T, Dirnagl U and Villringer A 1996 Cerebral oxygenation changes in response to motor stimulation *J. Appl. Physiol.* **81** 1174–83

Obrig H, Israel H, Kohl-Bareis M, Uludag K, Wenzel R, Müller B, Arnold G and Villringer A 2002 Habituation of the visually evoked potential and its vascular response implications for neurovascular coupling in the healthy adult *Neuroimage* **17** 1–18

Ogawa S, Tank D W, Menon R, Ellermann J M, Kim S G, Merkle H and Ugurbil K 1992 Intrinsic signal changes accompanying sensory stimulation functional brain mapping with magnetic resonance imaging *Proc. Natl Acad. Sci. USA* **89** 5951–5

Orfanidis S J 1996 *Optimum Signal Processing. An Introduction* 2nd edn (Englewood Cliffs, NJ: Prentice-Hall)

Pan J and Tompkins W J 1985 A real-time QRS detection algorithm *IEEE Trans. Biomed. Eng.* **32** 230–6

Re R, Contini D, Caffini M, Cubeddu R, Spinelli L and Torricelli A 2010 A compact time-resolved system for near infrared spectroscopy based on wavelength space multiplexing *Rev. Sci. Instrum.* **81** 113101

Riera J J and Sumiyoshi A 2010 Brain oscillations: ideal scenery to understand the neurovascular coupling *Curr. Opin. Neurol.* **23** 374–81

Roy C S and Sherrington C S 1890 On the regulation of the blood-supply of the brain *J. Physiol.* **11** 85–158.17

Sander T H, Liebert A, Burghoff M, Wabnitz H, Macdonald R and Trahms L 2007 Cross-correlation analysis of the correspondence between magnetoencephalographic and near-infrared cortical signals *Methods Inf. Med.* **46** 164–8

Sarter M and Turchi J 2002 Age- and dementia-associated impairments in divided attention: psychological constructs, animal models, and underlying neuronal mechanisms *Dement. Geriatr. Cogn. Disord.* **13** 46–58

Selb J, Stott J J, Franceschini M A, Sorensen A G and Boas D A 2005 Improved sensitivity to cerebral haemodynamics during brain activation with a time-gated optical system analytical model and experimental validation *J. Biomed. Opt.* **10** 11013

Sheth S A, Nemoto M, Guiou M, Walker M, Pouratian N and Toga A W 2004 Linear and nonlinear relationships between neuronal activity, oxygen metabolism, and haemodynamic responses *Neuron* **42** 347–55

Shibasaki H 2008 Human brain mapping haemodynamic response and electrophysiology *Clin. Neurophysiol.* **119** 731–43

Steinbrink J, Wabnitz H, Obrig H, Villringer A and Rinneberg H 2001 Determining changes in NIR absorption using a layered model of the human head *Phys. Med. Biol.* **46** 879–96

Syré F, Obrig H, Steinbrink J, Kohl M, Wenzel R and Villringer A 2003 Are VEP correlated fast optical signals detectable in the human adult by non-invasive nearinfrared spectroscopy (NIRS)? *Adv. Exp. Med. Biol.* **530** 421–31

Takahashi T, Takikawa Y, Kawagoe R, Shibuya S, Iwano T and Kitazawa S 2011 Influence of skin blood flow on near-infrared spectroscopy signals measured on the forehead during a verbal fluency task *Neuroimage* **57** 991–1002

Tanida M, Katsuyama M and Sakatani K 2007 Relation between mental stress-induced prefrontal cortex activity and skin conditions a near-infrared spectroscopy study *Brain Res.* **1184** 210–6

Tanida M, Sakatani K, Takano R and Tagai K 2004 Relation between asymmetry of prefrontal cortex activities and the autonomic nervous system during a mental arithmetic task nerainfrared spectroscopy study *Neurosci. Lett.* **36** 69–74

Telkemeyer S, Rossi S, Nierhaus T, Steinbrink J, Obrig H and Wartenburger I 2011 Acoustic processing of temporally modulated sounds in infants evidence from a combined near-infrared spectroscopy and EEG study *Front Psychol.* **1** 62

Thorn C E, Kyte H, Slaff D W and Shore A C 2011 An association between vasomotion and oxygen extraction *Am. J. Physiol. Heart Circ. Physiol.* **301** H442–9

Uludag K, Dubowitz D J, Yoder E J, Restom K, Liu T T and Buxton R B 2004 Coupling of cerebral blood flow and oxygen consumption during physiological activation and deactivation measured with fMRI *NeuroImage* **23** 148–55

Villringer A, Planck J, Stodieck S, Bötzel K, Schleinkofer L and Dirnagl U 1994 Noninvasive assessment of cerebral haemodynamics and tissue oxygenation during activation of brain cell function in human adults using near infrared spectroscopy *Adv. Exp. Med. Biol.* **345** 559–65

Wallois F, Mahmoudzadeh M, Patil A and Grebe R 2011 Usefulness of simultaneous EEG-NIRS recording in language studies *Brain Lang.* **121** 110–23

Zetterberg L H 1969 Estimation of parameters for a linear difference equation with application to EEG analysis *Math. Biosci.* **5** 227–75

Zimmermann P and Fimm B 1992 Handbuch der testbatterie zur Aufmerksamkeitsprüfung *Manual for the Attention Assessment Test* battery (Psytest, Herzogenrath)